JOC The Journal of Organic Chemistry

Article

pubs.acs.org/joc

Mechanisms and Reactivity Differences for Cycloaddition of Anhydride to Alkyne Catalyzed by Palladium and Nickel Catalysts: Insight from Density Functional Calculations

Hujun Xie,*[,†] Qiang Sun,[†] Gerui Ren,[†] and Zexing Cao*[,‡]

[†]Department of Applied Chemistry, Zhejiang Gongshang University, Hangzhou 310035, People's Republic of China

[‡]State Key Laboratory of Physical Chemistry of Solid Surfaces and Fujian Provincial Key Laboratory of Theoretical and Computational Chemistry, College of Chemistry and Chemical Engineering, Xiamen University, Xiamen 361005, People's Republic of China

Supporting Information

ABSTRACT: Mechanisms and reactivity differences for the cycloaddition of anhydride to alkyne catalyzed by the palladium and nickel catalysts have been investigated by extensive density functional theory (DFT) calculations. The predicted free energy profiles for the Pd- and Ni-catalyzed reactions have been used to evaluate possible mechanisms for the formation of different products. Calculations show that the formation of isocoumarin via the decarbonylative addition of anhydride to alkyne is kinetically more favorable than the channel to indenone in the Ni-catalyzed reaction. On the contrary, the preparation of naphthalene through sequential liberation of CO_2 and CO is kinetically more favorable than that the formation of indenone in the Pd-catalyzed process. The bonding differences between Pd−C and Ni−C bonds, arising from the relativistic effect of late transition metals, play an important role in regulating their catalytic activity. The calculation results show good agreement with the experiments.

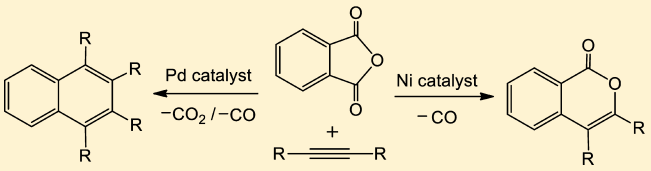

INTRODUCTION

Cycloadditions of anhydrides to unsaturated C−C bonds have attracted broad interest for their role in the production of more complicated polycyclic compounds.[1,2] Carboxylic anhydrides, as cheap, safe, and accessible reactants, are widely used in the transition-metal-catalyzed cross-coupling reactions. The oxidative addition of the carboxylic anhydride C−O bond via transition metals along with further CO or CO_2 extrusion is considered a useful method for the regioselective formation of C−C bonds.[3,4]

The transition-metal-catalyzed insertion reaction of an unsaturated C−C bond into a C−O bond of an oxacyclic compound is an important kind of direct transformation to afford more complicated oxacyclic compounds. Kurahashi et al.[5] developed the Ni-catalyzed cycloaddition of salicylic acid to alkynes via loss of ketone. The reaction mechanism was assumed to include the oxidative addition of an C−O bond to a Ni(0) complex. Subsequent elimination of benzophenone and coordination of alkyne yield a Ni(II) intermediate. The alkyne is then inserted into the Ni−C bond to form nickelacycle, which undergoes reductive elimination to yield the final product chromone.

Ni-catalyzed cycloadditions of thiophthalic anhydrides with alkynes to prepare substituted sulfur-containing heterocyclic compounds are also investigated.[6] It is demonstrated that these reactions can give three types of compounds selectively dependent on the experimental reaction conditions. The use of Ni(0)/PPr_3 catalyst in combination with Lewis acid can produce thioisocoumarin, and the use of Ni(0)/PCy_3 catalyst in this reaction can produce benzothiophene, while the use of Ni(0)/PMe_3 catalyst can generate thiochromone.

Kurahashi et al.[7] also studied the Ni-catalyzed [6−3 + 2] cycloaddition reactions of anthranilic acid derivatives with alkynes to give substituted indoles. The reaction mechanism consists of the oxidative addition of Ni(0) to an ester moiety, which allows intermolecular addition to alkynes by decarbonylation and 1,3-acyl migration. Yang et al.[8] studied the nickel-catalyzed decarboxylative cycloaddition of isatoic anhydrides with alkenes to prepare the tricyclic 2,3-dihydro-4-quinolones. Isatoic anhydrides react with various norbornenes to form the novel structure of quinolones. Kurahashi et al.[9] also reported decarbonylative cycloadditions of phthalimides with 1,3-dienes catalyzed by the nickel catalyst. It is noted that the cycloaddition proceeds regioselectively with respect to 1,3-dienes. Moreover, the regioselective cycloadditions of an unsymmetrically functionalized phthalimide with 1,3-dienes were also achieved.

The present cycloadditions exhibit excellent regio- and chemoselectivity in the presence of functional groups. Decarbonylative cycloaddition of phthalic anhydrides with allenes via the nickel catalyst is also reported.[10] The asymmetric variant of cycloaddition was also achieved by employing chiral

Special Issue: Mechanisms in Metal-Based Organic Chemistry

Received: July 18, 2014
Published: August 18, 2014

   dx.doi.org/10.1021/jo501618k | J. Org. Chem. 2014, 79, 11911−11921

phosphine ligands to provide δ-lactones enantioselectively. The reaction represents an unprecedented insertion reaction of C═C double bond into C−O bond. Meng et al.[11] investigated the nickel-catalyzed decarbonylative additions of anhydrides to alkynes by DFT calculations, and the insertion of alkynes into the Ni−C bond, prior to its insertion into the Ni−O bond, is predicted to be the rate-determining step for the whole catalytic cycle.

In addition, Kurahashi et al.[12] reported the nickel-catalyzed decarbonylative addition of phthalimides to alkynes. Further density functional theory (DFT) calculations by Cavallo et al.[13] showed that the reaction is initiated by the nickel insertion into the amide bond of the substrate to form the six-membered metallacycle. Subsequent decarbonylation takes place, which is followed by the insertion of the alkyne into the Ni−C (pyridine) bond. Finally, the reductive elimination occurs to give the final product. Here, the alkyne insertion is the rate-determining step. Kurahashi et al.[14] also attempted the Ni(0)-catalyzed decarboxylative carboamination of alkynes with isatoic anhydrides. Further DFT calculations by Sakaki et al.[15] showed that the catalytic reaction mechanism involves four steps, oxidative addition, decarboxylation, alkyne insertion, and reductive elimination. The facile decarboxylation is ascribed to the coordination of the N atom in isatoic anhydride to the Ni center, which can accelerate the decarboxylative step.

Recently, Kurahashi et al.[16] investigated the decarbonylative addition of anhydrides to alkynes by the nickel catalyst to generate isocoumarin, which has a wide range of biological activities.[17] The reaction mechanism has been proposed to consist of oxidative addition, decarbonylation, alkyne insertion, and reductive elimination. Jafarpour et al.[18] reported the Pd-catalyzed consecutive decarboxylative and decarbonylative addition of cyclic anhydrides to alkynes. This is the first case for the consecutive decarboxylative-decarbonylative cross coupling of cyclic anhydrides via a palladiumbenzyne intermediate.

Experimentally, enormous efforts have been made to develop the Pd and Ni catalysts for the addition of anhydride derivatives to alkynes. However, the product dependence on the Pd and Ni catalysts, as shown in Scheme 1, has not been well understood,

Scheme 1. Cycloaddition of Anhydrides to Alkynes by Palladium and Nickel Catalysts

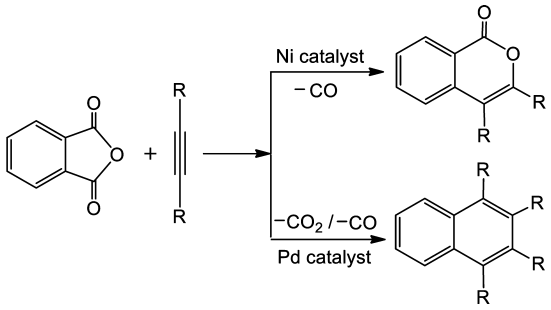

and the detailed reaction mechanisms are still elusive, since the intermediates are difficult to isolate for the present catalytic reactions. Herein, extensive DFT calculations have been used to explore the Pd- and Ni-catalyzed additions of anhydride derivatives to alkynes, and the activity differences between Ni and Pd catalysts, thermodynamic and dynamical properties of plausible reaction channels have been discussed and clarified.

COMPUTATIONAL DETAILS

All species in this study were fully optimized by means of the DFT calculations at the hybrid B3LYP level,[19] and this method has been successfully used in our previous studies[20] and other calculations on the Ni- and Pd-catalyzed reactions.[21] The 6-31G(d) basis set was used for the C, N, O and H atoms, while the effective core potentials (ECPs) of Hay and Wadt with a double-ζ valence basis set (LanL2DZ)[22] were selected to describe the Pd, Ni and Si atoms. Furthermore, the polarization functions of Pd(ζ_f) = 1.472,[23] Ni(ζ_f) = 3.130 and P(ζ_d) = 0.340 were added.[24] Frequency calculations have also been preformed to validate the stationary points as minima or transition states. To confirm the transition states indeed connecting two relevant minima, intrinsic reaction coordinate (IRC) calculations were also carried out.[25] All calculations were implemented via the Gaussian09 software package.[26]

In order to take the solvent effects into account, the conductor-like polarizable continuum model (CPCM)[27] was used for the single-point calculations based on the optimized geometries in the gas phase with the UAHF radii. For the Ni-catalyzed reaction, acetonitrile was selected as the solvent. While for the Pd-catalyzed reaction, *N,N*-dimethylformamide was selected as the solvent according to the experimental conditions.

It was well-known that the gas-phase calculations overestimate the entropic contribution to the Gibbs free energy for the reaction step with different numbers of reactant and product molecules in solution, and thus the reasonable corrections are necessary to add to the relative free energies according to the free volume theory.[28] For the 1:1 or 2:2 change, it is unnecessary to add the corrections. However, for the 2:1 (or 1:2) transformation, a correction of −2.6 (or 2.6) kcal/mol is required at the temperature of 298.15 K. These corrections have been validated in previous calculations.[29] In the present work, the relative free energies in the solvent were employed to evaluate the reaction mechanisms.

RESULTS AND DISCUSSION

According to previous experiments,[16,18] cycloadditions of anhydrides to alkynes catalyzed by Ni and Pd catalysts were described in Scheme 1. The results showed that different catalysts (Pd or Ni catalyst) can generate different products. Here, the plausible reaction mechanisms for the Pd- and Ni-catalyzed addition of anhydride derivatives to alkynes have been studied by DFT calculations, and the different reaction activities

Scheme 2. Proposed Ni-Catalyzed Cycle for the Decarbonylative Addition of Anhydride to Alkyne by Kurahashi et al.[16]

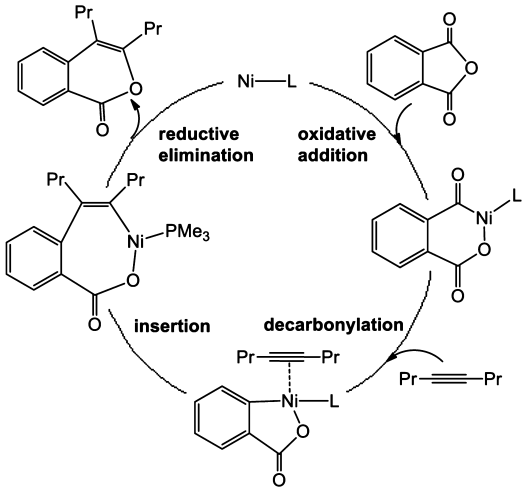

dx.doi.org/10.1021/jo501618k | J. Org. Chem. 2014, 79, 11911−11921

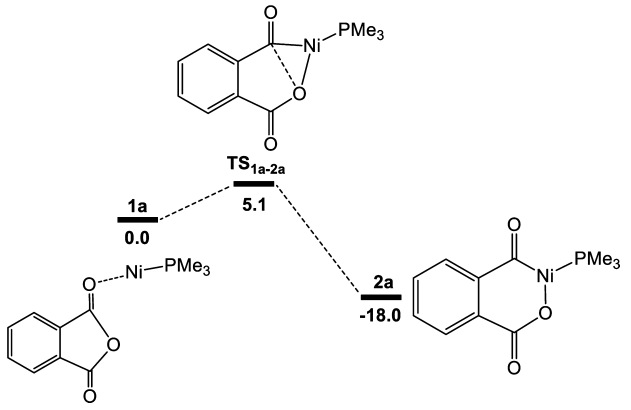

Figure 1. Free-energy profiles calculated for the oxidative addition step catalyzed by the Ni catalyst. The relative free energies in the solvent are given in kcal/mol.

between Ni and Pd catalysts have also been assessed and explored.

Ni-catalyzed decarbonylative addition of anhydride to alkyne. On the basis of experimental results, Kurahashi et al. proposed a reaction mechanism (Scheme 2),[16] including oxidative addition, decarbonylation, insertion, and reductive elimination, to account for the Ni-catalyzed decarbonylative addition of anhydride to alkyne for the formation of isocoumarin. The free energy profiles for the reaction are depicted in Figures 1−3, and the corresponding optimized structures are presented in Figures 4 and 5.

As shown in Figure 1, the coordination of anhydride to the Ni catalyst forms a two-coordinate Ni(0) complex **1a**. The reaction starts from the oxidative addition of anhydride O−C(=O) bond to the Ni(0) complex to give a six-membered acylnickel carboxylate metallacycle intermediate **2a**, and this step is obviously exergonic by 18.0 kcal/mol (Figure 1). The barrier is calculated to be only 5.1 kcal/mol from **1a** to $\mathbf{TS}_{1a-2a}$. From **2a**, there are two possible pathways for the following reaction, leading to the formation of different products. Path a comprises the initial decarbonylation followed by the alkyne insertion to generate isocoumarin (Figure 2). Path b initiates with the decarboxylation followed by the alkyne insertion to give indenone (Figure 3).

As shown in Figure 2, in path a, the complex **2a** proceeds through decarbonylation to afford a five-membered nickelacycle complex **3a**. This step is assisted by an interaction between the Ni atom and the closest aromatic carbon atom of the phenyl ring. The barrier is equal to 13.7 kcal/mol from **2a** to $\mathbf{TS}_{2a-3a}$, and the C−C bond in $\mathbf{TS}_{2a-3a}$ is computed to be 1.668 Å (Figure 4). From **3a**, two possible pathways for the alkyne insertion are identified (path ai and path aii). Path ai involves the alkyne insertion into the Ni−C bond to generate a seven-membered nickelacycle intermediate **5a**, where the CO_2 moiety is in trans-form with respect to the alkyne, whereas in path aii, the alkyne is inserted into the Ni−O bond to produce **9a** and the CO_2 moiety is adjacent to the alkyne, which is followed by

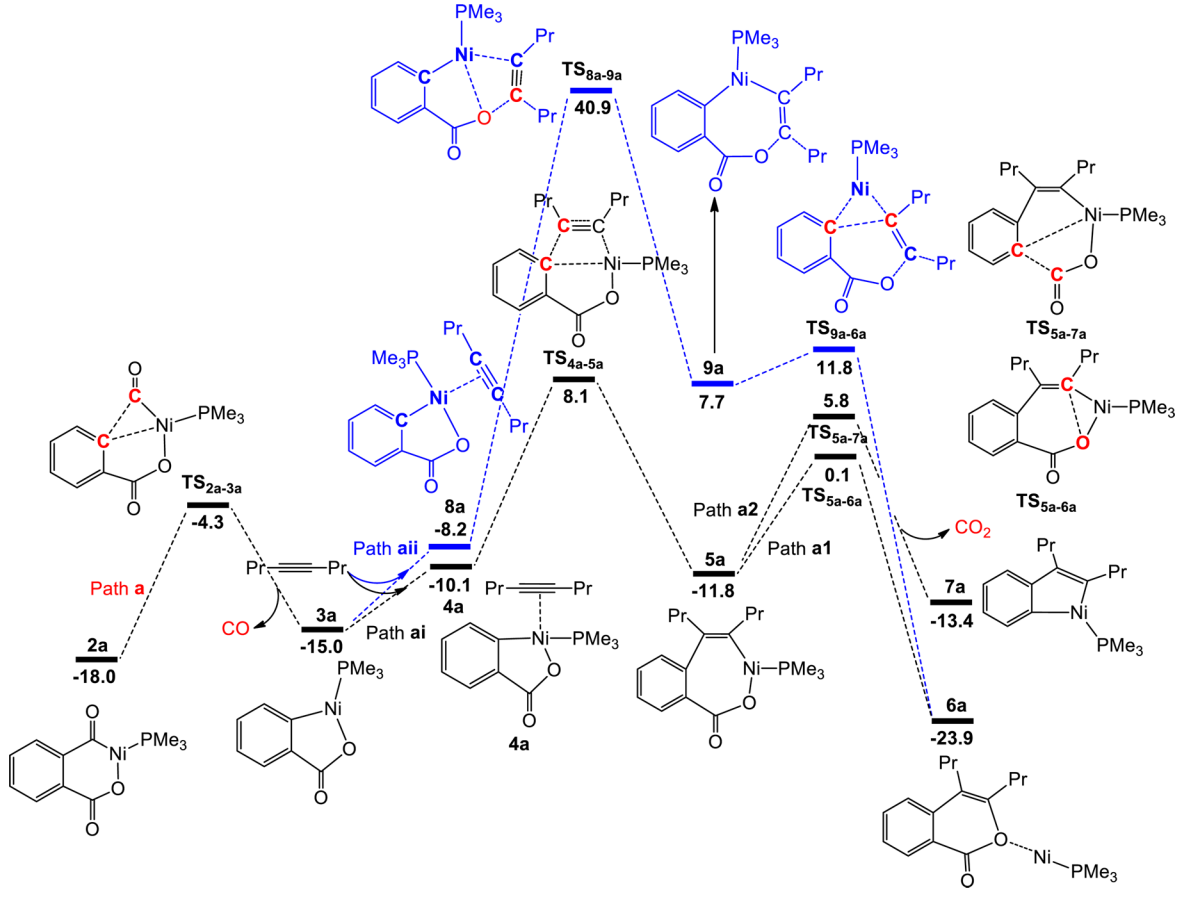

Figure 2. Free-energy profiles of path a involving the decarbonylative addition of anhydride to alkyne for the formation of isocoumarin. The relative free energies in the solvent are given in kcal/mol.

dx.doi.org/10.1021/jo501618k | J. Org. Chem. 2014, 79, 11911−11921

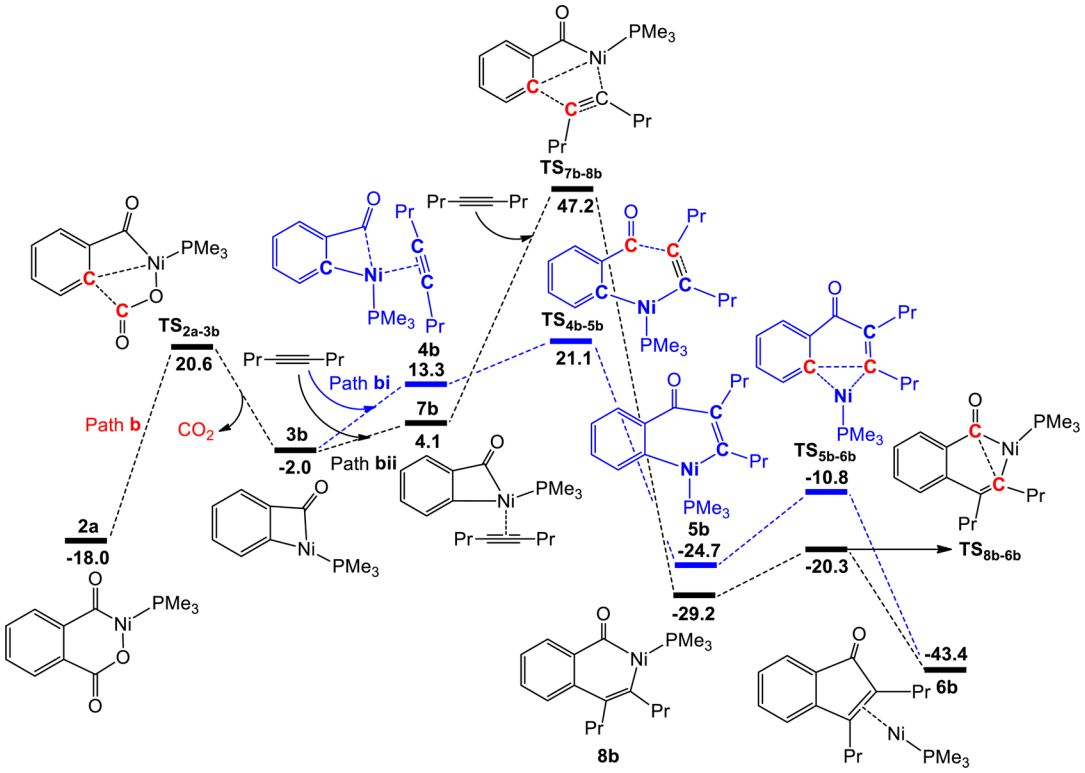

Figure 3. Free energy profiles of path b involving the decarboxylative addition of anhydride to alkyne for the formation of indenone. The relative free energies in the solvent are given in kcal/mol.

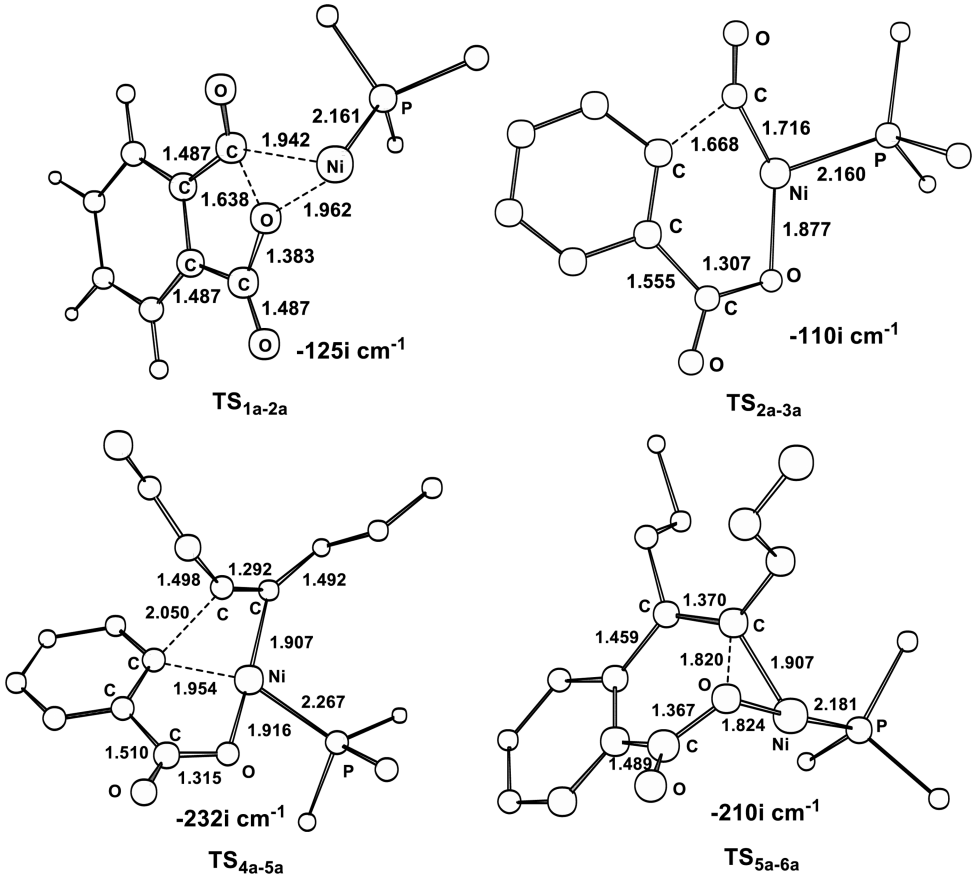

Figure 4. Optimized structures (Å) of selected transition states in Figures 1 and 2. All hydrogen atoms are omitted for clarity.

dx.doi.org/10.1021/jo501618k | J. Org. Chem. 2014, 79, 11911−11921

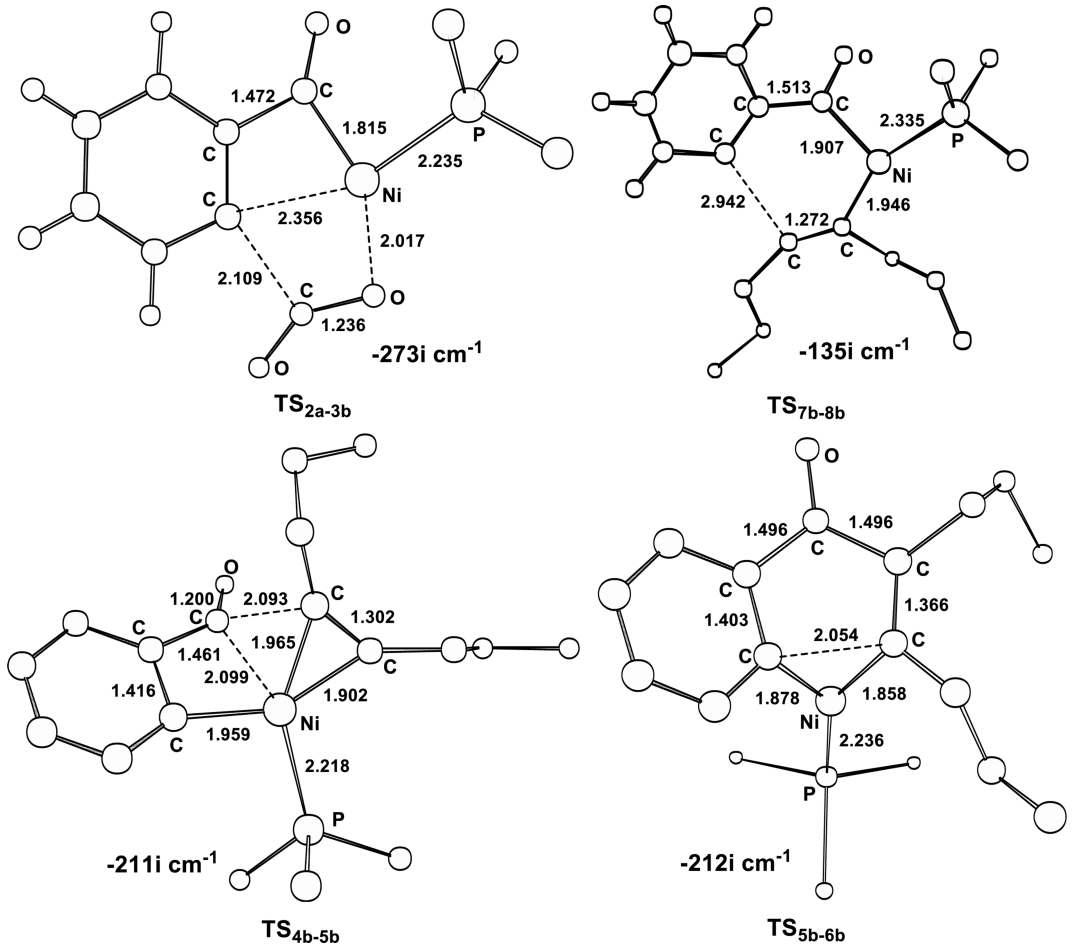

Figure 5. Optimized structures (Å) of selected transition states in Figure 3. All hydrogen atoms are omitted for clarity.

Scheme 3. Proposed Catalytic Cycle by Jafarpour et al.[18] for the Decarboxylative and Decarbonylative Addition of Cyclic Anhydrides to Alkynes by the Palladium Catalyst

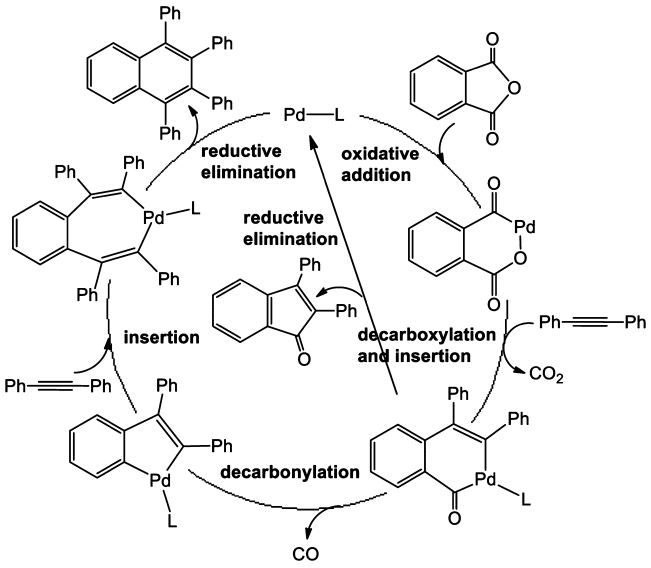

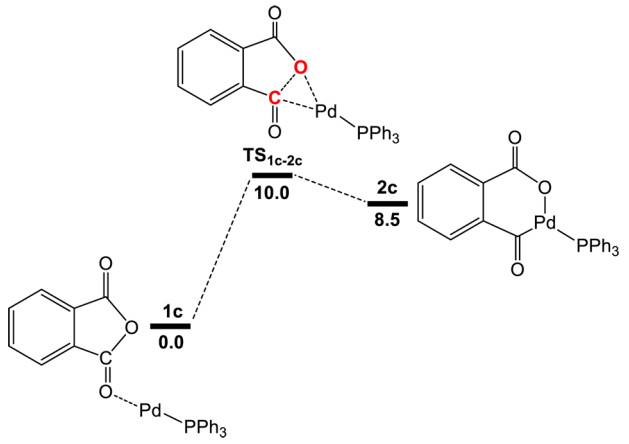

Figure 6. Free-energy profiles calculated for the Pd-catalyzed oxidative addition step. The relative free energies in the solvent are given in kcal/mol.

reductive elimination to yield the product **6a**. The calculations showed that path ai is kinetically more favorable than path aii. In path ai, the alkyne is coordinated to the Ni center of complex **3a** to provide the π-complex **4a**. Insertion of the alkyne proceeds to give **5a** with an overall free energy barrier of 26.1 kcal/mol from **2a** to TS_{4a-5a}, which is the rate-limiting step for the whole catalytic cycle. Previous calculations by Meng et al.[11] showed that the rate-determining free energy barrier for the alkyne insertion is calculated to be 37.5 kcal/mol. A five-coordinated transition state of nickel complex is involved in the alkyne insertion step, which is really rare for the nickel complex. Such high barrier suggests that the reaction is less possible at the experimental reaction temperature of 80 °C. From **5a**, two

dx.doi.org/10.1021/jo501618k | J. Org. Chem. 2014, 79, 11911−11921

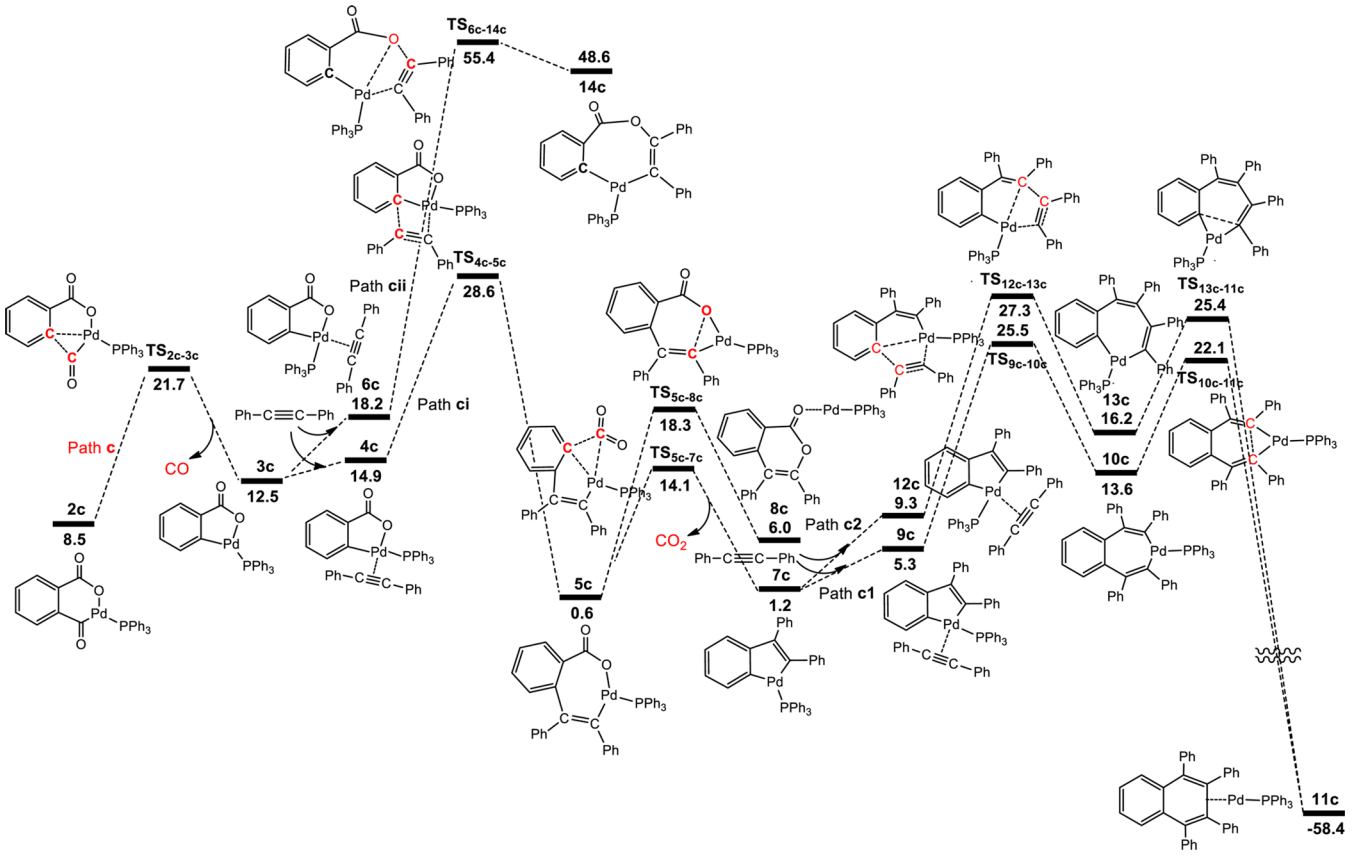

Figure 7. Free-energy profiles of path c involving the decarbonylative and decarboxylative addition of cyclic anhydride to alkyne catalyzed by the palladium catalyst. The relative free energies in the solvent are given in kcal/mol.

different pathways are outlined in Figure 2. Path a1 involves the C−O bond-forming reductive elimination to generate isocoumarin with a barrier of 11.9 kcal/mol ($\mathbf{TS}_{5a-6a}$). Path a2 considers the decarboxylation to give **7a** with a barrier of 17.6 kcal/mol ($\mathbf{TS}_{5a-7a}$). Accordingly, the reaction favors path a1 over path a2.

As depicted in Figure 3, the decarboxylation from the complex **2a** in path b takes place via the four-membered ring transition state ($\mathbf{TS}_{2a-3b}$). The predicted barrier is 38.6 kcal/mol from **2a** to $\mathbf{TS}_{2a-3b}$. The C−C separation in $\mathbf{TS}_{2a-3b}$ is calculated as 2.109 Å (Figure 5). The formation of complex **3b** is endergonic by 16.0 kcal/mol. From **3b**, two possible pathways are proposed for the formation of final products (paths bi and bii). Path bi involves the coordination of alkyne to the Ni center cis to the CO moiety to generate **4b**, and then alkyne inserts into the Ni−O bond to give **5b** via the transition state $\mathbf{TS}_{4b-5b}$, followed by the reductive elimination to give the desired product, while for path bii, the alkyne is coordinated to the Ni center trans to the CO moiety to produce **7b**. Then, the alkyne interts into the Ni−C bond to yield **8b**, followed by the reductive elimination to form the product **6b**. Taking into account of these results shown in Figure 3, we can clearly see that both paths bi and bii are kinetically unfavorable.[16]

As illustrated in Figure 2, the predicted low energy reaction pathway is consistent with the proposed mechanism by Kurahashi et al.,[16] containing oxidative addition, decarbonylation, insertion, and reductive elimination. Here, the insertion reaction is predicted to be the rate-determining step with the free energy spans of 26.1 kcal/mol from the complex **2a** to $\mathbf{TS}_{4a-5a}$ (Figure 2), which is also consistent with previous calculations.[11,13]

Pd-Catalyzed Consecutive Decarbonylative and Decarboxylative Addition of Cyclic Anhydride to Alkyne. Using the palladium catalyst in place of the nickel catalyst, the cycloaddition of anhydride to alkyne undergoes distinct reaction pathways to afford naphthalene derivatives. Here, we conducted the first theoretical study on this new kind of consecutive decarboxylative and decarbonylative cross coupling reaction, and possible mechanisms for the Pd-catalyzed addition of anhydride to alkyne have been explored by DFT calculations. Jafarpour et al.[18] proposed a mechanism for this reaction as shown in Scheme 3. Experiments revealed that the reaction mechanism involves the oxidative addition of palladium to the C−O bond, leading to the formation of acylpalladium carboxylate metallacycle. Subsequently, the insertion of alkynes takes place followed by CO_2 extrusion. Then CO is released followed by the insertion of the second alkyne. Finally, the reductive elimination occurs to give the product. Figures 6−8 describe the predicted free energy profiles for the formation of naphthalene derivatives. The corresponding optimized structures with selected structural parameters are presented in Figures 9 and 10.

As shown in Figure 6, from the complex **1c**, the oxidative addition of palladium to the anhydride C−O bond with a three-membered-ring transition state $\mathbf{TS}_{1c-2c}$ leads to the formation of acylpalladium carboxylate metallacycle **2c**, and the process is endergonic by 8.5 kcal/mol. The barrier for this step ($\mathbf{TS}_{1c-2c}$) is predicted to be 10.0 kcal/mol. From the complex **2c**, two possible pathways for the formation of final product are found.

dx.doi.org/10.1021/jo501618k | J. Org. Chem. 2014, 79, 11911−11921

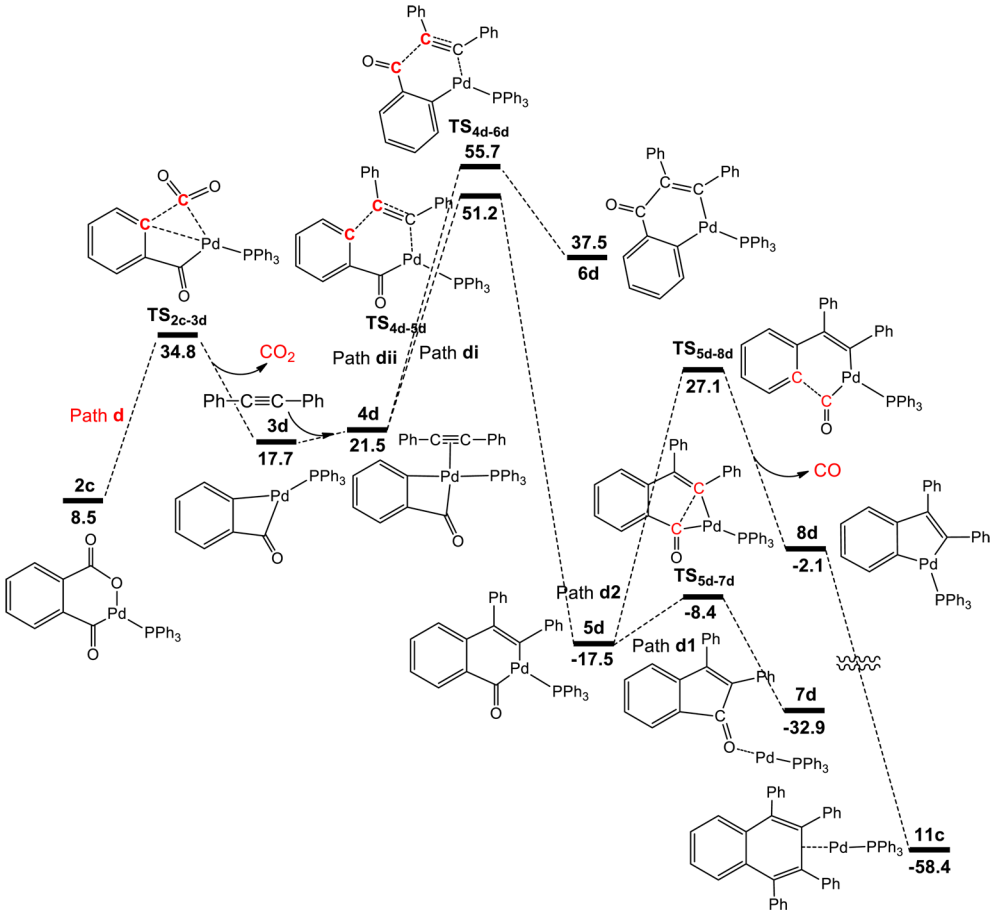

Figure 8. Free-energy profiles of path d involving the decarboxylative and decarbonylative addition of cyclic anhydride to alkyne catalyzed by the palladium catalyst. The relative free energies in the solvent are given in kcal/mol.

Path c involves the CO liberation prior to CO_2 extrusion (Figure 7), while path d considers the CO_2 liberation prior to CO extrusion (Figure 8). To discriminate between two competitive paths for CO_2 and CO releases, we have performed DFT calculations to explore the reaction mechanisms in detail.

A comparison of the predicted reaction pathways in Figures 7 and 8 reveals that path c is kinetically more favorable than path d. In path c, the CO extrusion occurs to give the five-membered palladacycle complex **3c**. A free energy barrier ($\mathbf{TS}_{\mathbf{2c-3c}}$) of 13.2 kcal/mol is required in this step, and the C−C distance in $\mathbf{TS}_{\mathbf{2c-3c}}$ is 1.817 Å (Figure 9). From **3c**, the alkyne insertion has two possible pathways. Path ci is related to the alkyne insertion into the Pd−C bond, while path cii comprises the alkyne insertion into the Pd−O bond. The calculations showed that path ci is kinetically more favorable than path cii. In path ci, the alkyne is coordinated to the palladium center trans to the CO_2 moiety to give a π-complex **4c**. Subsequently, the alkyne insertion into the Pd−C bond takes place with an overall free energy barrier of 28.6 kcal/mol from **1c** to $\mathbf{TS}_{\mathbf{4c-5c}}$, which is the rate-determining step for the whole catalytic cycle. The formation of intermediate **5c** is obviously exergonic by 14.3 kcal/mol.

From **5c**, the reaction can proceed via two possible pathways. One is related to the decarboxylation, and the other corresponds to the reductive elimination. Present calculations show that the decarboxylation is energetically more favorable with a barrier ($\mathbf{TS}_{\mathbf{5c-7c}}$) of 13.5 kcal/mol. The CO_2 moiety in $\mathbf{TS}_{\mathbf{5c-7c}}$ becomes almost perpendicular to the Pd-containing five-membered ring. In this step, the O−C−O angle increases to 139°, suggesting that the carboxyl group is changing to a free CO_2 molecule. The formation of an intermediate **7c** is slightly endergonic by 0.6 kcal/mol.

From **7c**, there are two possible pathways for the second alkyne insertion. Path c1 involves the alkyne insertion into the aryl−palladium bond, and path c2 comprises the alkyne insertion into the Pd−C(alkyne). On the basis of the present calculations, path c1 is kinetically more favorable than path c2. In path c1, the alkyne is coordinated to the palladium center trans to the first alkyne carbon atom to give **9c**. Subsequently, the reaction proceeds via the second alkyne insertion to generate **10c**, followed by the reductive elimination to yield **11c**. The barrier ($\mathbf{TS}_{\mathbf{10c-11c}}$) for the reductive elimination is calculated to be 8.5 kcal/mol and the C−C bond distance in $\mathbf{TS}_{\mathbf{10c-11c}}$ is 2.100 Å (Figure 9). Finally, the naphthalene derivative is produced and the complex **1c** is regenerated for the next catalytic cycle.

On the basis of the computational results discussed above, a revised version of the reaction cycle is given in Scheme 4. The mechanism includes four major stages: (1) the oxidative addition of Pd(0) to the C−O bond to generate the acylpalladium carboxylate metallacycle **2c**; (2) the decarbonylation followed by the first alkyne insertion into the aryl-nickel bond; (3) the decarboxylation followed by the second alkyne insertion into the aryl−nickel bond; (4) the reductive elimination occurs to give the products of naphthalene derivatives and regenerate the complex **1c**. The first alkyne

dx.doi.org/10.1021/jo501618k | J. Org. Chem. 2014, 79, 11911−11921

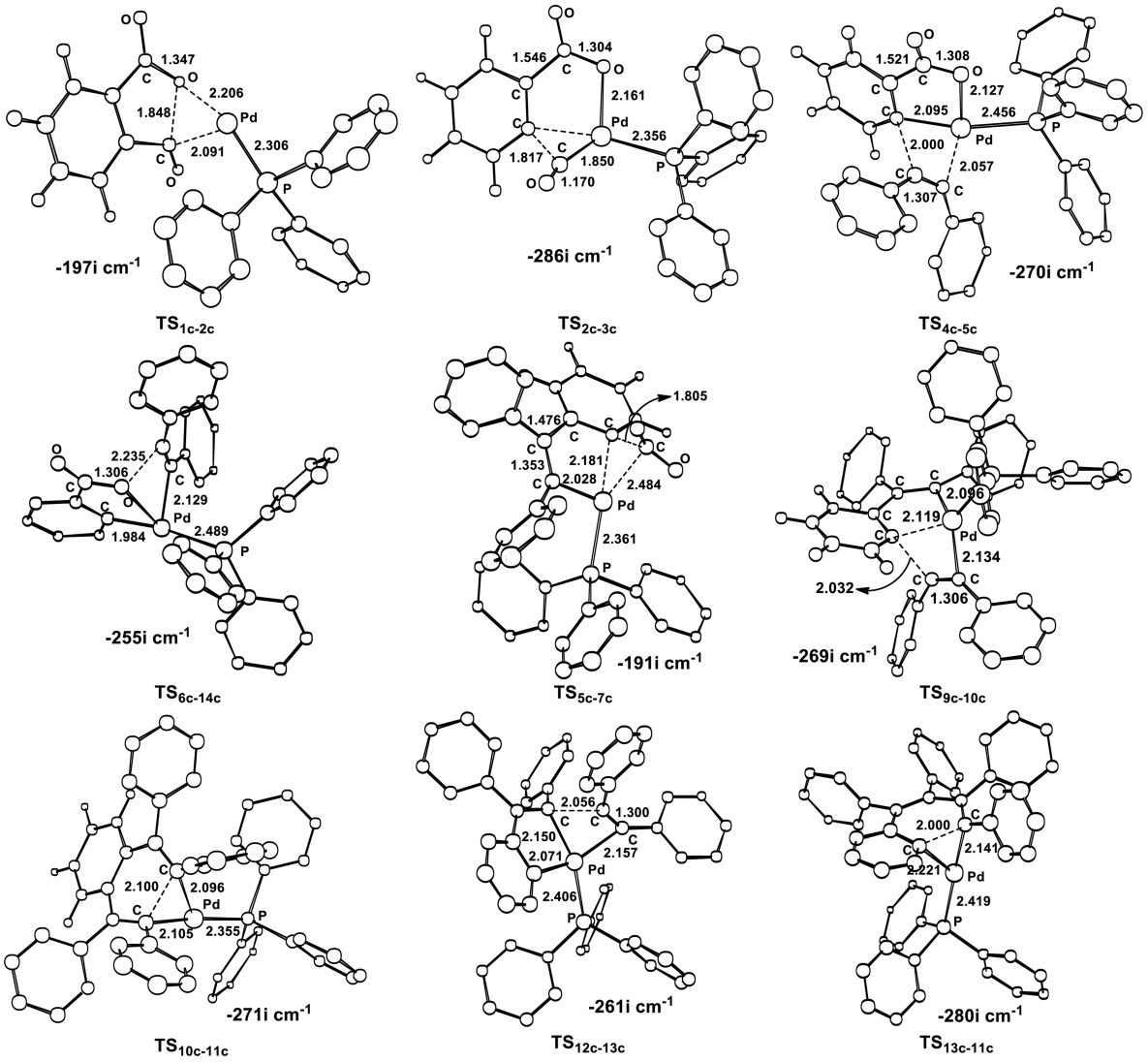

Figure 9. Optimized structures (Å) of selected transition states in Figures 6 and 7. All hydrogen atoms are omitted for clarity.

insertion step is rate-limiting and requires the free energy spans of 28.6 kcal/mol from **1c** to $\mathbf{TS}_{4c-5c}$ (Figure 7). These results also suggest that the loss of CO prior to the CO_2 extrusion is more favorable both thermodynamically and dynamically, differing from the proposed mechanism by Jafarpour et al.[18]

Here, the ligand modification effect on both Pd and Ni catalysts has been also investigated. Calculations show that the key steps are less influenced by the ligand modification. For the nickel catalysts, the barriers for the alkyne insertion ($\mathbf{TS}_{4a-5a}$, after decarbonylation) are calculated to be 26.1 and 27.8 kcal/mol for the Ni−PMe_3 and Ni−PPh_3 catalysts, respectively, and the barriers for the alkyne insertion ($\mathbf{TS}_{4b-5b}$, after decarboxlation) are predicted to be 39.1 and 41.7 kcal/mol for the Ni−PMe_3 and Ni−PPh_3 catalysts, respectively. For the palladium catalysts, the barriers for the decarbonylation ($\mathbf{TS}_{2c-3c}$) are calculated to be 13.2 and 14.5 kcal/mol for the Ni−PMe_3 and Ni−PPh_3 catalysts, respectively. And the barriers for the decarboxlation ($\mathbf{TS}_{2c-3d}$) are predicted to be 26.3 and 28.7 kcal/mol for the Ni−PMe_3 and Ni−PPh_3 catalysts, respectively. Generally, the use of relatively small ligands may reduce the barrier by about 2 kcal/mol, which can be ascribed to the steric effects of different ligands on the formation of transition states.

Comparison of Ni- and Pd-Catalytic Activities. On the basis of the present calculations, for the Ni catalyst, path ai (Figure 2) to the formation of isocoumarin is kinetically more favorable than path b to the formation of indenone (Figure 3), while for the use of the palladium catalyst the formation of naphthalene (path c1 in Figure 7) is kinetically more favorable than that of indenone (path d1 in Figure 8). All computational results are in accordance with the experimental observations.[16,18]

We investigated the Ni-catalyzed decarbonylative addition of anhydride to alkyne. The calculations showed that the decarbonylation step experiences a barrier of 13.7 kcal/mol ($\mathbf{TS}_{2a-3a}$ in Figure 2), while the decarboxylation step has a substantially higher barrier of 38.6 kcal/mol ($\mathbf{TS}_{2a-3b}$ in Figure 3), indicating that the decarbonylation should be prior to the decarboxylation in the catalytic reaction. The relatively high barrier of decarboxylation may be ascribed to instability of the intermediate **3b** due to the ring strain of four-membered ring (Ni−C−C−C). In addition, we can see from Figure 2, starting from the intermediate **5a**, the reductive elimination ($\mathbf{TS}_{5a-6a}$ in path a1) involved in the formation of isocoumarin is more favorable than decarboxylation ($\mathbf{TS}_{5a-7a}$ in path a2), both kinetically and thermodynamically.

dx.doi.org/10.1021/jo501618k | J. Org. Chem. 2014, 79, 11911−11921

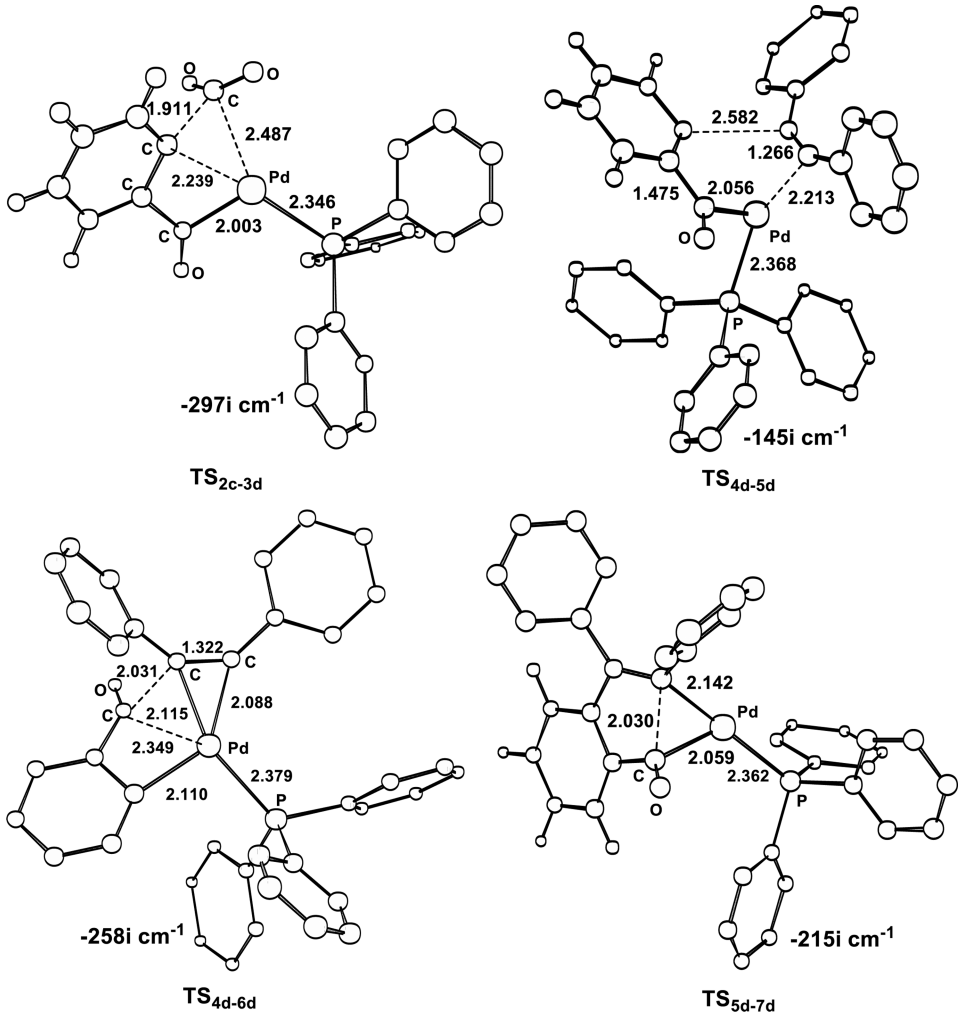

Figure 10. Optimized structures (Å) of selected transition states in Figure 8. All hydrogen atoms are omitted for clarity.

Scheme 4. Revised Catalytic Cycle for the Decarboxylative and Decarbonylative Addition of Cyclic Anhydrides to Alkynes by the Palladium Catalyst

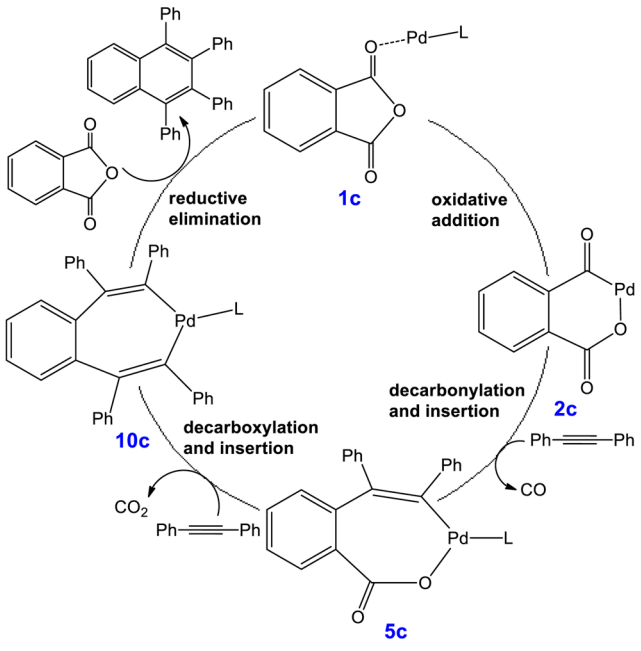

We also consider the decarbonylative and decarboxylative addition of anhydride to alkyne catalyzed by the palladium catalyst. The calculation results demonstrated that the decarbonylation step (21.7 kcal/mol for $\mathbf{TS}_{2c-3c}$ in path c) is more favorable than the decarboxylation step (34.8 kcal/mol for $\mathbf{TS}_{2c-3d}$ in path **d**). These results are in good agreement with the Ni-catalyzed decarbonylative addition of anhydride to alkyne with the decarbonylation prior to the decarboxylation.

Clearly, we can see that there are quite different activities between the Ni and Pd catalysts as observed in experiments. Starting from **5c**, the Pd-catalyzed decarboxylation (13.5 kcal/mol for $\mathbf{TS}_{5c-7c}$) is more favorable than the reductive elimination (17.7 kcal/mol for $\mathbf{TS}_{5c-8c}$), both thermodynamically and dynamically. On the contrary, the Ni-catalyzed reductive elimination (11.9 kcal/mol for $\mathbf{TS}_{5a-6a}$) is energetically more favorable than the decarboxylation (17.6 kcal/mol for $\mathbf{TS}_{5a-7a}$). Such a difference in activity can be ascribed to the remarkable relativistic effects of late transition metals. Previous calculations show that the relativistic effect of late transition metals may play an important role in the metal−carbon bonding, which makes the Pd−C bond much stronger than the Ni−C bond.[30] Accordingly, the Pd-catalyzed decarboxylation step involving the Pd−C bond formation is energetically more favorable than the corresponding Ni-catalyzed process. In addition, the bonding differences among metal−carbon bonds also modify the relative stabilities between the products from

dx.doi.org/10.1021/jo501618k | J. Org. Chem. 2014, 79, 11911−11921

the reductive elimination and decarboxylation in the Ni- and Pd-catalytic processes. In particular, for the Ni catalyst, **6a** from the reductive elimination is more stable than **7a** from the decarboxylation, while for the Pd catalyst **7c** from the decarboxylation is more stable than **8c** from the reductive elimination. Here, the coordination interactions between oxygen and metal also contribute the relative stability to some extent. According to the theory of hard−soft acid−base,[31] the hard oxygen ligand prefers the relatively hard Ni over the soft Pd, and thus the product **6a** from the reductive elimination is quite stable.

CONCLUSIONS

DFT calculations have been performed to elucidate the detailed mechanisms for the Ni- and Pd-catalyzed cycloaddition of anhydride to alkyne. The free-energy profiles along possible alternative reaction pathways have been estimated to have insight into the relative energetics and reactivity. For the nickel catalyst, the computational results show that the formation of isocoumarin via the decarbonylative addition of anhydride to alkyne is kinetically more favorable than the indenone channel. The calculated mechanism is consistent with a catalytic cycle proposed by Kurahashi et al.,[16] which basically includes four stages: (1) the oxidative addition of anhydride C−O bond to yield an acylpalladium intermediate **2a**, (2) the decarbonylation to form the intermediate **3a** followed by the alkyne insertion to give **4a**, (3) the alkyne insertion to produce a seven-membered nickelacycle intermediate **5a**, and (4) the reductive elimination to afford the complex **6a**, with the isocoumarin release and the active species regeneration. The alkyne insertion was predicted to be the rate-determining step with the free energy spans of 26.1 kcal/mol.

For the palladium catalyst, the formation of naphthalene via sequential liberation of CO_2 and CO is kinetically more favorable than that of indenone. The present results argue against the previously proposed mechanism. The revised reaction mechanism for the Pd-catalyzed consecutive decarboxylative and decarbonylative addition of anhydride to alkyne consist of four steps: (1) the oxidative addition of the Pd(0) center to afford an acylpalladium carboxylate metallacycle **2c**; (2) the decarbonylation takes place followed by the first alkyne insertion into the aryl-palladium bond to give a seven-membered palladacycle complex **5c**; (3) the decarboxylation occurs, followed by the second alkyne insertion into the arylpalladium bond to yield **10c**; (4) the reductive elimination to give naphthalene derivatives and regenerate the complex **1c**. The calculations show that the first alkyne insertion is the rate-limiting step for the whole catalytic cycle and the catalytic reaction has an overall free energy barrier of 28.6 kcal/mol from **1c** to $\mathbf{TS}_{\mathbf{4c-5c}}$. In addition, the loss of CO is prior to CO_2 extrusion in the low energy reaction pathway. The remarkable catalytic activity differences between Ni and Pd catalysts observed in experiments can be ascribed to the relativistic effect of late transition metals on the metal−carbon bonding. The present calculations provide new insights into the catalytic mechanisms for the transition-metal-catalyzed cycloaddition of anhydrides to alkynes.

ASSOCIATED CONTENT

Supporting Information

Cartesian coordinates of the optimized structures involved in the catalytic processes. This material is available free of charge via the Internet at http://pubs.acs.org.

AUTHOR INFORMATION

Corresponding Authors

*E-mail: hujunxie@gmail.com. Tel: (+86)-592-2186081.
*E-mail: zxcao@xmu.edu.cn. Tel: (+86)-592-2186081.

Notes

The authors declare no competing financial interest.

ACKNOWLEDGMENTS

This work was supported by the National Science Foundation of China (21203166, 21373164, and 21133007) and the Ministry of Science and Technology (2011CB808504 and 2012CB214900).

REFERENCES

(1) (a) Russell, G. A.; Myers, C. L.; Bruni, P.; Neugebauer, F. A.; Blankespoor, R. *J. Am. Chem. Soc.* **1970**, *92*, 2762. (b) Chapman, O. L.; McIntosh, C. L.; Pacansky, J. *J. Am. Chem. Soc.* **1973**, *95*, 4061. (c) Dushin, R. G.; Danishefsky, S. J. *J. Am. Chem. Soc.* **1992**, *114*, 655. (d) Shibuya, I.; Gama, Y.; Shimizu, M.; Goto, M. *Heterocycles* **2002**, *57*, 143. (e) Holloway, G. A.; Hugel, H. M.; Rizzacasa, M. A. *J. Org. Chem.* **2003**, *68*, 2200.

(2) (a) Leardini, R.; Franco Pedulli, G.; Tundo, A.; Zanardi, G. *J. Chem. Soc., Chem. Commun.* **1985**, 1390. (b) Yue, D.; Larock, R. C. *J. Org. Chem.* **2002**, *67*, 1905. (c) Benati, L.; Calestani, G.; Leardini, R.; Minozzi, M.; Nanni, D.; Spagnolo, P.; Strazzari, S.; Zanardi, G. *J. Org. Chem.* **2003**, *68*, 3454. (d) Nakamura, I.; Sato, T.; Yamamoto, Y. *Angew. Chem., Int. Ed.* **2006**, *45*, 4473. (e) Tseng, N.-W.; Lautens, M. *J. Org. Chem.* **2009**, *74*, 1809.

(3) (a) Johnson, J. B.; Rovis, T. *Acc. Chem. Res.* **2008**, *41*, 327. (b) Yamamoto, A. *J. Organomet. Chem.* **2004**, *689*, 4499. (c) Zapf, A. *Angew. Chem., Int. Ed.* **2003**, *42*, 5394. (d) Goo*β*en, L. J.; Koley, D.; Hermann, H. L.; Thiel, W. *Organometallics* **2006**, *25*, 54. (e) Xin, B.; Zhang, Y.; Cheng, K. *J. Org. Chem.* **2006**, *71*, 5725. (f) Goo*β*en, L. J.; Ghosh, K. *Angew. Chem., Int. Ed.* **2001**, *40*, 3458.

(4) (a) Myers, A. G.; Tanaka, D.; Mannion, M. R. *J. Am. Chem. Soc.* **2002**, *124*, 11250. (b) Zhang, S. L.; Fu, Y.; Shang, R.; Guo, Q. X.; Liu, L. *J. Am. Chem. Soc.* **2010**, *132*, 638. (c) Li, Z.; Jiang, Y. Y.; Yeahley, A. A.; Bour, J. P.; Liu, L.; Chruma, J.J.; Fu, Y. *Chem.—Eur. J.* **2012**, *18*, 14527.

(5) Ooguri, A.; Nakai, K.; Kurahashi, T.; Matsubara, S. *J. Am. Chem. Soc.* **2009**, *131*, 13194.

(6) Inami, T.; Baba, Y.; Kurahashi, T.; Matsubara, S. *Org. Lett.* **2011**, *12*, 1912.

(7) Maizuru, N.; Inami, T.; Kurahashi, T.; Matsubara, S. *Org. Lett.* **2011**, *13*, 1206.

(8) Sun, M.; Ma, Y. N.; Li, Y. M.; Tian, Q. P.; Yang, S. D. *Tetrahedron Lett.* **2013**, *54*, 5091.

(9) Fujiwara, K.; Kurahashi, T.; Matsubara, S. *Org. Lett.* **2010**, *12*, 4548.

(10) Ochi, Y.; Kurahashi, T.; Matsubara, S. *Org. Lett.* **2011**, *13*, 1374.

(11) Meng, Q. X.; Li, M. *J. Mol. Model.* **2013**, *19*, 4545.

(12) Kajita, Y.; Matsubara, S.; Kurahashi, T. *J. Am. Chem. Soc.* **2008**, *130*, 6058.

(13) Poater, A.; Vummaleti, S. V. C.; Cavallo, L. *Organometallics* **2013**, *32*, 6330.

(14) Yoshino, Y.; Kurahashi, T.; Matsubara, S. *J. Am. Chem. Soc.* **2009**, *131*, 7494.

(15) Guan, W.; Sakaki, S.; Kurahashi, T.; Matsubara, S. *Organometallics* **2013**, *32*, 7564.

(16) Kajita, Y.; Kurahashi, T.; Matsubara, S. *J. Am. Chem. Soc.* **2008**, *130*, 17226.

(17) Agata, N.; Nogi, H.; Milhollen, M.; Kharbanda, S.; Kufe, D. *Cancer Res.* **2004**, *64*, 8512. (b) Pochet, L.; Frederick, R.; Masereel, B. *Curr. Pharm. Design* **2004**, *10*, 3781.

(18) Jafarpour, F.; Hazrati, H.; Nouraldinmousa, S. *Org. Lett.* **2013**, *15*, 3816.

(19) (a) Becke, A. D. *J. Chem. Phys.* **1993**, *98*, 5648. (b) Lee, C.; Yang, W.; Parr, R. G. *Phys. Rev. B* **1988**, *37*, 785. (c) Becke, A. D. *J. Chem. Phys.* **1993**, *98*, 1372. (d) Becke, A. D. *Phys. Rev. B* **1988**, *38*, 3098.
(20) (a) Xie, H. J.; Zhao, L. J.; Yang, L.; Lei, Q. F.; Fang, W. J.; Xiong, C. H. *J. Org. Chem.* **2014**, *79*, 4517. (b) Yang, L.; Ren, G. R.; Ye, X. C.; Que, X. Y.; Lei, Q. F.; Fang, W. J.; Xie, H. J. *J. Phys. Org. Chem.* **2014**, *27*, 237. (c) Xie, H. J.; Zhang, H.; Lin, Z. Y. *Organometallics* **2013**, *32*, 2336. (d) Xie, H. J.; Lin, F. R.; Lei, Q. F.; Fang, W. J. *Organometallics* **2013**, *32*, 6957. (e) Xie, H. J.; Zhang, H.; Lin, Z. Y. *New J. Chem.* **2013**, *37*, 2856. (f) Xie, H. J.; Lin, F. R.; Yang, L.; Chen, X. S.; Ye, X. C.; Tian, X.; Lei, Q. F.; Fang, W. J. *J. Organomet. Chem.* **2013**, *745*−*746*, 417. (g) Xie, H. J.; Lin, F. R.; Lei, Q. F.; Fang, W. J. *J. Phys. Org. Chem.* **2013**, *26*, 933.
(21) (a) Tang, S. Y.; Guo, Q. X.; Fu, Y. *Chem.—Eur. J.* **2011**, *49*, 13866. (b) Perez-Rodriguez, M.; Braga, A. A. C.; de Lera, A. R.; Maseras, F.; Alvarez, R.; Espinet, P. *Organometallics* **2010**, *29*, 4983. (c) Surawatanawong, P.; Hall, M. B. *Organometallics* **2008**, *27*, 6222. (d) Lam, K. C.; Marder, T. B.; Lin, Z. Y. *Organometallics* **2010**, *29*, 1849. (e) Xue, L. Q.; Lin, Z. Y. *Chem. Soc. Rev.* **2010**, *39*, 1692. (f) Yu, H. Z.; Fu, Y.; Guo, Q. X.; Lin, Z. Y. *Organometallics* **2009**, *28*, 4507. (g) Zheng, W. X.; Ariafard, A.; Lin, Z. Y. *Organometallics* **2008**, *27*, 246. (h) Lam, K. C.; Marder, T. B.; Lin, Z. Y. *Organometallics* **2007**, *26*, 758. (i) Ariafard, A.; Lin, Z. Y. *J. Am. Chem. Soc.* **2006**, *128*, 13010.
(22) (a) Check, C. E.; Faust, T. O.; Bailey, J. M.; Wright, B. J.; Gilbert, T. M.; Sunderlin, L. S. *J. Phys. Chem. A* **2001**, *105*, 8111. (b) Hay, P. J.; Wadt, W. R. *J. Chem. Phys.* **1985**, *82*, 299.
(23) Ehlers, A. W.; Bohme, M.; Dapprich, S.; Gobbi, A.; Hollwarth, A.; Jonas, V.; Kohler, K. F.; Stegmann, R.; Veldkamp, A.; Frenking, G. *Chem. Phys. Lett.* **1993**, *208*, 111.
(24) Huzinaga, S. *Gaussian Basis Sets for Molecular Calculations*; Elsevier Science Pub. Co.: Amsterdam, 1984.
(25) (a) Fukui, K. *J. Phys. Chem.* **1970**, *74*, 4161. (b) Fukui, K. *Acc. Chem. Res.* **1981**, *14*, 363.
(26) Gaussian 09, Revision A.1: Frisch, M. J.; Trucks, G.. W.; Schlegel, H. B.; Scuseria, G. E.; Robb, M. A.; Cheeseman, J. R.; Scalmani, G.; Barone, V.; Mennucci, B.; Petersson, G. A.; Nakatsuji, H.; Caricato, M.; Li, X.; Hratchian, H. P.; Izmaylov, A. F.; Bloino, J.; Zheng, G.; Sonnenberg, J. L.; Hada, M.; Ehara, M.; Toyota, K.; Fukuda, R.; Hasegawa, J.; Ishida, M.; Nakajima, T.; Honda, Y.; Kitao, O.; Nakai, H.; Vreven, T.; Montgomery, J. A., Jr.; Peralta, J. E.; Ogliaro, F.; Bearpark, M.; Heyd, J. J.; Brothers, E.; Kudin, K. N.; Staroverov, V. N.; Kobayashi, R.; Normand, J.; Raghavachari, K.; Rendell, A.; Burant, J. C.; Iyengar, S. S.; Tomasi, J.; Cossi, M.; Rega, N.; Millam, J. M.; Klene, M.; Knox, J. E.; Cross, J. B.; Bakken, V.; Adamo, C.; Jaramillo, J.; Gomperts, R.; Stratmann, R. E.; Yazyev, O.; Austin, A. J.; Cammi, R.; Pomelli, C.; Ochterski, J. W.; Martin, R. L.; Morokuma, K.; Zakrzewski, V. G.; Voth, G. A.; Salvador, P.; Dannenberg, J. J.; Dapprich, S.; Daniels, A. D.; Farkas, O.; Foresman, J. B.; Ortiz, J. V.; Cioslowski, J.; Fox, D. J. Gaussian, Inc., Wallingford, CT, 2009.
(27) Barone, V.; Cossi, M. *J. Phys. Chem. A* **1998**, *102*, 1995. (b) Cossi, M.; Rega, N.; Scalmani, G.; Barone, V. *J. Comput. Chem.* **2003**, *24*, 669.
(28) Benson, S. W. *The Foundations of Chemical Kinetics*; Krieger Publishing Co.: Malabar, FL, 1982.
(29) (a) Okuno, Y. *Chem.—Eur. J.* **1997**, *3*, 212. (b) Ardura, D.; López, R.; Sordo, T. L. *J. Phys. Chem. B* **2005**, *109*, 23618. (c) Schoenebeck, F.; Houk, K. N. *J. Am. Chem. Soc.* **2010**, *132*, 2496. (d) Liu, Q.; Lan, Y.; Liu, J.; Li, G.; Wu, Y. D.; Lei, A. *J. Am. Chem. Soc.* **2009**, *131*, 10201. (e) Wang, M. Y.; Fan, T.; Lin, Z. Y. *Organometallics* **2012**, *31*, 560. (f) Wang, M. Y.; Fan, T.; Lin, Z. Y. *Polyhedron* **2012**, *32*, 35. (g) Liu, B. W.; Gao, M.; Dang, L.; Zhao, H. T.; Marder, T. B.; Lin, Z. Y. *Organometallics* **2012**, *31*, 3410.
(30) (a) Heinemann, C.; Hertwig, R. H.; Wesendrup, R.; Koch, W.; Schwarz, H. *J. Am. Chem. Soc.* **1995**, *117*, 495. (b) Cao, Z. X. Reactivity of Metal Carbene Clusters $Pt_nCH_2^+$ and $PtMCH_2^+$ (M = Cu, Ag, Au, Pt, Rh) Toward O_2 and NH_3: A Computational Study. In *Computational Organometallic Chemistry*; Wiest, O., Wu, Y., Eds.; Springer-Verlag: Berlin, 2012; pp 169−218.
(31) (a) Pearson, R. G. *J. Am. Chem. Soc.* **1963**, *85*, 3533. (b) Pearson, R. G. *J. Chem. Educ.* **1968**, *45*, 581. (c) Pearson, R. G. *J. Chem. Educ.* **1968**, *45*, 643.